NASA Contractor Report 4200

Development of Three-Dimensional Code for the Analysis of Jet Mixing Problem

Part I: Laminar Solution

Khaled S. Abdol-Hamid

CONTRACT NAS1-18599
DECEMBER 1988

NASA

NASA Contractor Report 4200

Development of Three-Dimensional Code for the Analysis of Jet Mixing Problem

Part I: Laminar Solution

Khaled S. Abdol-Hamid
Analytical Services and Materials, Inc.
Hampton, Virginia

Prepared for
Langley Research Center
under Contract NAS1-18599

National Aeronautics
and Space Administration

Scientific and Technical
Information Division

1988

ABSTRACT

Future aircraft will eventually feature nonaxisymmetric or rectangular nozzles. Developing a three-dimensional code to simulate the characteristics of the jet exhaust plume, issuing from nonaxisymmetric nozzles, in general, at different flight conditions, is very important. In the present investigation, two three-dimensional codes were developed to simulate the shock-cell structure of circular nozzles. These codes are used to solve the parabolized and simplified Navier-Stokes equations respectively. Both codes are based on a method previously developed by Newsome et al. (Ref. 1). These codes are fully vectorized on the VPS 32 at NASA Langley Research Center. The axisymmetric underexpanded supersonic jet flow problem, exhausting into still air, was used as a test case for developing an efficient three-dimensional code which should be capable of simulating two-dimensional problems and preserving crossplane symmetry of the flow downstream of the jet exit.

INTRODUCTION

Future propulsion systems for fighter aircraft must be designed for maximum maneuverability over a wide range of flight Mach numbers (Ref. 2 and 3). These features can be achieved with rectangular or nonaxisymetric nozzles (Ref. 4-8). Rectangular nozzles provide more rapid plume velocity decay than axisymetric nozzles (circular jet) and is simpler to modify, for example, to incorporate thrust vectoring (Ref. 9). Developing an efficient computational technique is essential to fully understanding the flow characteristics of these nozzles (rectangular nozzles). This computational technique should have a three-dimensional calculation capability and be able to simulate a wide range of jet flow conditions.

One of the most popular techniques for computing supersonic jet flows is a space marching scheme based on solving the steady, parabolized Navier-Stokes (PNS) equations. The principle advantage of the PNS approach is its greater computational efficiency compared to that of methods which solve the full unsteady Navier-Stokes equations. The efficiency results from the fact that a solution can be obtained by a spatial marching approach in which the solution is advanced downstream from some specified initial condition. Thus, for steady supersonic flows, only a single marching sweep is needed.

At the present time, a few such codes are available for predicting such flows, but they are limited in calculation capabilities. Dash and Wolf developed a two-dimensional (SCIPVIS (Ref. 10)) and a three-dimensional (SCIP3D Ref. 11)) parabolized Navier-Stokes code for analyzing propulsive jet mixing problems. SCIPVIS solves the mean flow equations for steady-state, two-dimensional compressible flows. This code can quantitively predict many of the details of the shock-cell structure, the turbulent mixing with an external stream, and the subsequent decay of the shock-cell strength as the result of shock/mixing-layer interactions. The SCIPVIS code can also give accurate predictions for underexpanded and overexpanded cases. SCIP3D solves the mean flow equations for steady-state, three-dimensional compressible flows. Wolf et al. (Ref. 12) have used SCIP3D to simulate an axisymetric supersonic jet problem. They found that, SCIP3D code overpredicted the shock-cell decay and spacing as compared with the SCIPVIS result. These comparisons indicate that further work and modifications in SCIP3D code are required to duplicate SCIPVIS result. They recommended the use of time-iterative procedure in plane to plane basis to replace their noniterative methodology which is proven to be very complex to deal with. They also suggested that the governing equation

should be formulated in generalized coordinates form, which will simplify the solution procedure for arbitrary exit shapes.

In this study, an underexpanded supersonic jet will be used as a test case for developing the present three-dimensional code. The shock-cell structure in underexpanded, supersonic jets has been the subject of several experimental and theoretical studies in recent years (Ref. 13-17). An understanding of these structures is especially important to the field of aeroacoustics where shocks contribute significantly to jet noise (Ref. 13). A schematic of a typical flow field for an underexpanded, supersonic jet is given in fig. 1. The jet is characterized by repetitive shock cells whose strength and size are modified through turbulent mixing with the surrounding medium.

The objective of the present study is the application and comparisons of two recently developed codes to simulate the shock-cell structure of the underexpanded supersonic jet problem. These codes were developed by modifying the 3D code developed by Newsome et al. (Ref. 1). Their code was used to solve the thin layer Navier-Stokes equations for a laminar, hypersonic afterbody flow problem. On the other hand, the present codes will be used in solving the Thin-layer Navier-Stokes (TLNS) and the Parabolized Navier-Stokes (PNS) equations for laminar or turbulent jet flow problems. Different options were added to the original code. These options are as follows:

1. Either half (one symmetry; HP) or quarter (two symmetry plane; QP) of the cross-flow plane can be simulated. The QP option can be useful in calculating square or circular jets.
2. Van Leer's Flux Vector Splitting method or Rao's Flux Differencing technique can be used to calculate the flux in the subsonic and supersonic regions of the flow.

3. A limiter can be used in the shock region, thus eliminating overshoots or undershoots.
4. The state variables at cell interface is constructed from either the primative or conservative variables.

The present codes use an implicit, approximately-factored, upwind, flux splitting finite volume algorithm. The flux-splitting and upwind spatial differencing method for the convection terms, used in the present study, has several advantages over central difference schemes. This method has natural numerical dissipation and better stability property. Both codes are third order accuracy in the cross-plane directions and second order in the streamwise direction. These codes solve the equations in conservation form for a generalized coordinate system. The paper will also discuss some of the differences in computational requirements between the PNS and NS codes.

GOVERNING EQUATIONS

The TLNS equations can be written in the following generalized coordinate and conservative form:

$$\frac{\partial \hat{Q}}{\partial t} + \frac{\partial \hat{E}}{\partial \xi} + \frac{\partial \hat{F}}{\partial \eta} + \frac{\partial \hat{G}}{\partial \zeta} = 0 \tag{1}$$

where

$$\hat{Q} = \frac{Q}{J}$$

$$\hat{E} = S_x E_i + S_y F_i + S_z G_i = \hat{E}_i$$

$$\hat{F} = R_x(E_i - E_v) + R_y(F_i - F_v) + R_z(G_i - G_v) = \hat{F}_i + \hat{F}_v$$

$$\hat{G} = T_x E_i + T_y F_i + T_z G_i = \hat{G}_i$$

S_x, S_y, S_z, R_x, R_y, R_z, T_x, T_y and T_z are the components of the surface normals. These terms and the cell volume, Vol, are evaluated using the procedures described by Chakravarthy and Szema (Ref. 19).

The inviscid (convection) flux vectors of the TLNS equations are given by

$$F_i = (\rho v, \rho uv, \rho v^2 + p, \rho vw, (E_t + p)v)^T$$

$$G_i = (\rho w, \rho uw, \rho vw, \rho w^2 + p, (E_t + p)w)^T \qquad (2)$$

where the total energy is

$$E_t = \frac{P}{\gamma - 1} + \frac{1}{2}(u^2 + v^2 + w^2)\rho$$

The viscous (diffusion) flux vector are of the form

$$E_v = (0, \tau_{xx}, \tau_{xy}, \tau_{xz}, u\tau_{xx} + v\tau_{xy} + w\tau_{xz} - q_x)^T$$

$$F_v = (0, \tau_{xy}, \tau_{yy}, \tau_{yz}, u\tau_{xy} + v\tau_{yy} + w\tau_{yz} - q_y)^T \qquad (3)$$

$$G_v = (0, \tau_{xz}, \tau_{yz}, \tau_{zz}, u\tau_{xz} + v\tau_{yz} + w\tau_{zz} - q_z)^T$$

where the viscous stress and heat transfer terms are given by

$$\tau_{xx} = \frac{2}{3}\mu\left(2\frac{\partial u}{\partial x} - \frac{\partial v}{\partial y} - \frac{\partial w}{\partial z}\right) \qquad \tau_{xy} = \mu\left(\frac{\partial u}{\partial y} + \frac{\partial v}{\partial x}\right) \qquad q_x = \frac{\mu}{(\gamma - 1)\,Pr}\frac{\partial a^2}{\partial x}$$

$$\tau_{yy} = \frac{2}{3}\mu\left(2\frac{\partial v}{\partial y} - \frac{\partial u}{\partial x} - \frac{\partial w}{\partial z}\right) \qquad \tau_{yz} = \mu\left(\frac{\partial u}{\partial z} + \frac{\partial w}{\partial x}\right) \qquad q_y = \frac{\mu}{(\gamma - 1)\,Pr}\frac{\partial a^2}{\partial y}$$

$$\tau_{zz} = \frac{2}{3}\mu\left(2\frac{\partial w}{\partial z} - \frac{\partial u}{\partial x} - \frac{\partial v}{\partial y}\right) \qquad \tau_{yz} = \mu\left(\frac{\partial v}{\partial z} + \frac{\partial w}{\partial y}\right) \qquad q_z = \frac{\mu}{(\gamma - 1)\,Pr}\frac{\partial a^2}{\partial z}$$

The Parabolized Navier-Stokes (PNS) equations are obtained from the TLNS equations when the unsteady terms are omitted. If a space-marching procedure is used to solve these equations, the following assumptions should be enforced (Ref. 20):

1. The streamwise velocity component is, everywhere, greater than zero
2. The pressure gradient term in the streamwise direction $(\frac{\partial p}{\partial \xi})$ is either omitted or treated with other technique to avoid a complex eigenvalue.

In this study, the technique of Vingeron et. al. (Ref. 20) is adopted to supress the departure solutions associated with the elliptic behaviour of the equations. Vingeron et al. (Ref. 20) show that PNS equations is hyperbolic-parabolic provided that

$$\hat{E}_i = [\rho\hat{U},\ \rho u\hat{U} + S_x\omega p,\ \rho v\hat{U} + S_y\omega p,\ \rho\omega\hat{U} + S_z\omega p,\ (E_t + p)\hat{U}]^T \qquad (4)$$

where

$$\omega = 1 \qquad M_\xi > 1$$

$$= \frac{\sigma\gamma M_\xi^2}{1 + (\gamma - 1)\, M_\xi^2} \qquad M_\xi < 1$$

σ is a safety factor for not taking into account the nonlinearity of the governing equations.

COMPUTATIONAL METHOD

In this section, the implicit upwind/relaxation algorithm is used to solve the unsteady Navier-Stokes equation. The laws of conservation of mass, momentum, and energy over a volume, Vol, bounded by a surface S, can be expressed in integral form as

$$\frac{\partial}{\partial t} \int_{Vol} \hat{Q} dV + \int_S (\bar{\bar{H}} \quad n) dS = 0 \tag{5}$$

The tensor $\bar{\bar{H}}$ can be written in terms of the Cartesian fluxes by

$$\bar{\bar{H}} = (\hat{E}_i - \hat{E}_v)i + (\hat{F}_i - \hat{F}_v)j + (\hat{G}_i - \hat{G}_v)k$$

Associating the subscripts j,k,l with ξ, η, ζ directions, a numerical approximation to Eq. (5) may be written in the following form:

$$(\hat{Q}_{j,k,l})_t + \hat{E}_{j+\frac{1}{2},\,k,\,l} - \hat{E}_{j-\frac{1}{2},\,k,\,l}$$

$$+ \hat{F}_{j,k+\frac{1}{2},\,l} - \hat{F}_{j,k-\frac{1}{2},\,l} \tag{6}$$

$$+ \hat{G}_{j,k,l+\frac{1}{2}} - \hat{G}_{j,k,l,\frac{1}{2}} = 0$$

where $\hat{E}$, $\hat{G}$ and $\hat{F}$ are numerical fluxes at the boundary sides of the cell and $\hat{Q}$ is the cell-average value for the numerical approximation to $\bar{Q}$.

The flux vectors ($\hat{E}$, $\hat{F}$ and $\hat{G}$) are split according to the scheme of Van Leer (Ref. 21). These fluxed are split according to their contravariant Mach number

(M_ξ, M_η and M_ζ), defined as

$$M_\xi = \frac{\bar{U}}{a},\ M_\eta = \frac{\bar{V}}{a} \text{ and } M_\zeta = \frac{\bar{W}}{a} \tag{7}$$

where

$$\bar{U} = (S_x u + S_y v + S_z w)/S$$

$$\bar{V} = (R_x u + R_y v + R_z \omega)/R$$

$$\bar{W} = (T_x u + T_y v + T_z \omega)/T$$

$$S^2 = S_x^2 + S_y^2 + S_z^2$$

$$R^2 = R_x^2 + R_y^2 + R_z^2 \qquad \text{and } T^2 = T_x^2 + T_y^2 + T_z^2$$

As an example, for supersonic flow in the ξ direction

$$\hat{E}^{+} = \hat{E}\,, \qquad \hat{E}^{-} = 0\,, \qquad M_{\xi} \geq 1$$

$$\hat{E}^{+} = 0\,, \qquad \hat{E}^{-} = \hat{E}\,, \qquad M_{\xi} \leq -1 \tag{8}$$

and for subsonic flow $-1 \leq M_{\xi} \leq 1$

$$\hat{E}^{\pm} = S \begin{Bmatrix} E^{\pm}_{mass} \\ E^{\pm}_{mass}\,\{S_x(-\bar{U} \pm 2a)/\gamma S + u\} \\ E^{\pm}_{mass}\,\{S_y(-\bar{U} \pm 2a)/\gamma S + v\} \\ E^{\pm}_{mass}\,\{S_z(-\bar{U} \pm 2a)/\gamma S + w\} \\ E^{\pm}_{energy} \end{Bmatrix}$$

where

$$E^{\pm}_{mass} = \pm\rho a\,(M_{\xi} \pm 1)^2/4$$

$$E^{\pm}_{energy} = E^{\pm}_{mass}\,\{-(\gamma - 1)\,\bar{U}^2 \pm 2(\gamma - 1)\bar{U}\,a + 2\,a^2\}/(\gamma^2 - 1) + \tag{10}$$

$$\frac{1}{2}\,(u^2 + v^2 + w^2)$$

The flux at (n + 1) is linearized as

$$\hat{E}^{n+1} = \hat{E}^{n} + \left(\frac{\partial \hat{E}}{\partial Q}\right)^{n} \Delta Q$$

Now, the flux difference is written as

$$\begin{aligned}
\hat{E}^{n+1}_{j+\frac{1}{2},k,l} - \hat{E}^{n+1}_{j-\frac{1}{2},k,l} &= \left\{\hat{E}^{+}(Q^{-}) + \hat{E}^{-}(Q^{+})\right\}^{n}_{j+\frac{1}{2},k,l} \\
&\quad - \left\{\hat{E}^{+}(Q^{-}) + \hat{E}^{-}(Q^{+})\right\}^{n}_{j-\frac{1}{2},k,l} \\
&\quad + \left\{\frac{\partial \hat{E}^{+}(Q^{-})}{\partial Q}\Delta Q^{-} + \frac{\partial \hat{E}^{-}(Q^{+})}{\partial Q}\Delta Q^{+}\right\}_{j+\frac{1}{2},k,l} \\
&\quad - \left\{\frac{\partial \hat{E}^{+}(Q^{-})}{\partial Q}\Delta Q^{-} + \frac{\partial \hat{E}^{-}(Q^{+})\,\Delta Q^{+}}{\partial Q}\Delta Q^{+}\right\}_{j-\frac{1}{2},k,l}
\end{aligned} \tag{11}$$

The conserved variables Q^{+}, Q^{-} obtained by an upwind biased one parameter family

$$\begin{aligned}
Q^{-}_{j+\frac{1}{2},k,l} &= Q_{j,k,l} + \frac{\phi}{4}\left\{(1-k_{\xi})\nabla_{\xi} + (1+k_{\xi})\Delta_{\xi}\right\}Q_{j,k,l} \\
Q^{+}_{j+\frac{1}{2},k,l} &= Q_{j+1,k,l} - \frac{\phi}{4}\left\{(1+k_{\xi})\nabla_{\xi} + (1-k_{\xi})\Delta_{\xi}\right\}Q_{j,k,l}
\end{aligned} \tag{12}$$

where

$$\Delta_{\xi}Q_{j,k,l} = Q_{j+1,k,l} - Q_{j,k,l}, \quad \nabla_{\xi}Q_{j,k,l} = Q_{j,k,l} - Q_{j-1,k,l}$$

$\phi = 0$ first order fully upwind

$K_\xi = -1$, $\phi = 1$ second order fully upwind

$K_\xi = \frac{1}{3}$, $\phi = 1$ third order biased upwind

However, to ensure Montone interpolation for the third order interpolation in the vicinity of a shock, a min mod limiter is used as follows:

$$\nabla Q = \text{min mod } (\nabla Q, b\Delta Q)$$

$$\Delta Q = \text{min mod } (\Delta Q\ ,\ b\nabla Q) \qquad (13)$$

where b is a compression parameter, $b = \frac{3 - k_\xi}{1 - k_\xi}$

It should be mentioned that the upwind split-flux difference procedure are only used for the inviscid convection parts of the flux vectors ($\hat{F}$ & $\hat{G}$). A second order, central difference is used to represent the diffussion terms of SNS and PNS equations.

In the present study, first order upwind method is used to evaluate the implicit (Jacobian part of equation (11)). This will result in great reduction of the computational steps and will not affect the steady-state accuracy which is controlled by the R.H.S. of the equation. Equation (6) can be written as

$$\frac{I}{\Delta t}\,\text{Vol} + B_\xi + B_\eta + B_\zeta\ \Delta Q^{n+1}$$

$$+ A_\xi \Delta Q^{n+1}_{j-1} + A_\eta \Delta Q^{n+1}_{k-1} + A_\zeta \Delta Q^{n+1}_{l-1}$$

$$+ C_\xi \Delta Q^{n+1}_{j+1} + C_\eta \Delta Q^{n+1}_{k+1} + C_\zeta \Delta Q^{n+1}_{l+1} = R.H.S^n$$

$$A_\xi = (J_1^+)_{j-\frac{1}{2}}, \quad B_\xi = (J_1^+)_{j+\frac{1}{2}} - (J_1^-)_{j-\frac{1}{2}}, \quad C_\xi = (J_1^-)_{j+\frac{1}{2}}$$

$$A_\eta = (J_2^+)_{k-\frac{1}{2}} - V_2\,(k-\tfrac{1}{2}, k-1),$$

$$B_\eta = (J_2^+)_{k+\frac{1}{2}} - (J_2^-)_{k-\frac{1}{2}} + V_z(k+\tfrac{1}{2}, k) - V_2(k-\tfrac{1}{2}, k)$$

$$C_\eta = (J_2^-)_{k+\frac{1}{2}} - V_2\,(k+\tfrac{1}{2}, k+1)$$

$$A_\zeta = (J_3^+)_{l-\frac{1}{2}}$$

$$B_\zeta = J_3^+\ _{l+\frac{1}{2}} + (J_3^-)_{l-\frac{1}{2}}$$

$$C_\zeta = (J_3^-)_{l+\frac{1}{2}}$$

$$\{p_f,\ u_f\ v_f,\ w_f\ ,\ \rho_f\}^T_\eta = \{p,\ -u,v,w,\rho\}_{\zeta_0,\eta}$$

These relations are equivalent to set the gradient of ρ, v, w and E and the value of u to zero along ζ_0 line.

3) Conditions at ζ_{max}

Factitious grid points are located along the side of ζ_{max} line as shown in figure (3). For the quarter plane (QP) simulation, the values of the factitious points are

$$\{p_f,\ u_f,\ v_f,\ w_f,\ \rho_f\}^T_\eta = \{p,\ u,\ -\ v,\ w,\ \rho\}^T_{\zeta_{max},\ \eta}$$

4) Condition at the centerline η_0 or $\eta = 0.$ $(x = 0.$ and $y = 0.)$

Factitious points are added across the η_0 line as shown in figure (3). Their values are evaluated as follows:

QP simulation

$$\{p_f\ u_f\ v_f\ w_f\ \rho_f\}^T_{\zeta_f} = \{p,\ -\ u,\ -v,\ w,\ \rho\}^T_{\zeta,1} \qquad \begin{matrix} \zeta_f = \zeta_{max},\ 1 \\ \zeta = 1,\ \zeta_{max} \end{matrix}$$

HP simulation

$$\{p_f,\ u_f,\ v_f,\ w_f,\ \rho_f\}^T_\zeta = \{p_,\ -\ u,\ v,\ w,\ \rho\}^T_{\zeta,1}$$

5) Conditions on the Far-Field Boundary

a) $\eta = \eta_{max}$

The treatment of this boundary is based on Rieman invarients for a one-dimensional flow.

Riemann invarients

$$\hat{P} = \bar{V}_{\eta_{max}} + \frac{2}{\gamma - 1} a_{\eta_{max}}$$

$$\hat{N} = \bar{V}_{\infty} - \frac{2}{\gamma - 1} a_{\infty}$$

where,

$$\bar{V} = r_x u + r_y v + r_z w \qquad \{r\}_{\eta_{max}} \equiv \{r\}_{\infty} = \frac{1}{R} \{R_x, R_y, R_z\}$$

then,

$$\bar{V}_R = \frac{1}{2} (\hat{P} + \hat{N})$$

$$a_R = \frac{\gamma - 1}{4} (\hat{P} - \hat{N})$$

Inflow Boundary, $\bar{V}_R < o$

$$\{p,u,v,w,\rho\}^T_{\eta_{max}+1} = \{p,u,v,w,\rho\}^T_{\infty} + \bar{V}_R \{o,r_x,r_y,r_z,o\}^T$$

Outflow Boundary, $\bar{V}_R >, 0$

$$\{P,u,v,w,\rho\}^T_{\eta_{max}+1} = \{\frac{\gamma P}{a_R^2}, u,v,w,\rho\}^T_\infty + (\bar{V}_R - \bar{V}_{\eta_{max}}) \{o,r_x,r_y,r_z,o\}^T$$

b) ξ_{max}

This boundary is treated as the same as in 5-a where the surface normal r is replaced by s in the above calculations. These calculations are, only, used for the subsonic portion of the flow, whereas first order extrapolation was used for the supersonic part.

RESULTS AND DISCUSSIONS

In this section, the present three-dimensional codes are used to predict the shock-cell decay and flow characteristics of an underexpanded supersonic jet (1. < M < 2.) issued into still air. The three-dimensional results are, then, compared with the predicted results using a two-dimensional PNS code (SCIPVIS (Ref. 10) as well as the experimental data of Norum and Seiner (Ref. 16) exhausting into nominally still air. It should be mentioned that PNS techniques assume that the velocity in the streamwise direction always has a non-negative value. Norum and Shearin (Ref. 22) investigate the shock structure and noise of supersonic jets in simulated flight to Mach 0.4. They show that the changes in shock strength and amplitude of broadband shock noise in flight to Mach 0.4 are insignificant. Therefore, all calculations presented in this paper are for an external stream at a Mach number of 0.05. Comparisons are presented for static pressure distributions measured along the jet centerline.

Two test cases were selected for comparison:

1. Underexpanded, cold-air, supersonic jet -M = 2.0, p/p = 1.45.
2. Underexpanded, cold-air, sonic jet - M = 1.0, p/p = 1.62

In the present PNS calculations,

1. The jet starts with a top-hat profile at x = 0.
2. The local time-like iteration is activated at j-plane for n-iteration until the R.H.S. of the equation (15) is reduced to four-order of magnitude from its original value.
3. The solution at j is used as an initial condition for the j + 1-plane which, in turn, reduce the number of iterations required to reach converged solution at J + 1-plane.
4. Step 2 and 3 are repeated for all j-planes. Both test cases are converged within a number of interations less than 70. The PNS solutions are used as an initial condition for the TLNS solution as suggested by Walter et al. This approach will reduce the number of globel iteration required for the TLNS to reach a steady state solution.

To get a good insight of the capability of each code using less computer resource (memory and time), we have selected a coarse grid in the T-direction to predict the shock-cell structure of the Mach 2 jet. The Quarter-Plane option will be sufficient in solving axisymmetric problems. A typical grid distribution is shown in figure 2 with 160x61x11 (JxKxL) grid. It is believed that the highest gradient (pressure, temperature, and streamwise velocity), in the i-direction occurs close to the sonic-line (sonic-surface for 3-D case). In this investigation, the location of the sonic-line is always less than 1.5 jet-radii from the jet centerline. Based on these observations, a fine grid

was used for 1.5 jet-radii and stretched grid up to jet-radii. On the other hand, a uniform grid was used in the ξ-direction.

Case 1 - M = 2.0, P/P = 1.45

In figure (4), the measured centerline static pressure illustrates the decaying shock structure that occurs as a result of the interaction of the shocks with the growing mixing layer. The jet is operated at a pressure ratio of 1.45 which corresponds to a fully expanded Mach number of 2.24 and is issued from a convergent-divergent nozzle with a design Mach number of 2. Figure (5) shows the comparison between the results predicted using PNS and TLNS code for the streamwise pressure variation along the jet centerline. The PNS predictions were completed in 240 CPU seconds compared to 8400 CPU seconds used by the TLNS code. This comparison shows that the PNS code is quite efficient, as compared to TLNS code, in predicting the shock-cell structure of this case. Figure (6) shows the comparison between the pressure and density contour, respectively, using PNS and TLNS code. In this figure, the PNS is able to give essentially the same result presented by the TLNS code. However, the TLNS code gives a better description for the compression and expansion (reflected and intercepting) shocks for the whole flow domain than the one given by the PNS solution which gives good description for the first 5 shock cells.

Figure (7) shows the calculating centerline pressure using 160, 320 and 640 grid points in the streamwise direction respectively. This comparison shows that increasing the grid refinement in the steamwise direction does not have a significant effect in the predictions of shock-cell spacing (number of shock-cell) however, it does show improvement in the strength and shape of the first three shock-cell (in particular the first reflected shock).

Finally, figure (8) shows the comparisons between 3-D and 2-D PNS solution with the measured streamwise pressure variation along the jet centerline. The measure static pressure distributions illustrate the decaying shock structure that occurs due to the interaction of the shocks with the growing mixing layer. Both the PNS solutions predict the pressure variations up through the first 4 shock cells and underestimate the rest of shock-cell decay. This was expected as the mixing layer and turbulent dissipation of the shock strength are not modeled in both codes. This problem can be resolved by using an adequate turbulence model.

Case 2 - M = 1.0, P/P = 1.61

The experimental results shown in figure (9) are for the underexpanded condition (Pj/Pa = 1.61) for a sonic nozzle. This pressure ratio corresponds to a fully expanded Mach number of 1.37, and this figure shows that the measured data appear to decay abruptly after the fourth shock cell. Although there are no flow-field data available to explain this uncharacteristic rapid decay, acoustic data obtained under similar conditions suggested that such phenomena may be caused by acoustic resonance. Figure (10) shows the results predicted with the 3-D and 2-D PNS codes compared with measured centerline pressures. Both calculations show reasonably good agreement up through the first 4 shock cells, although there is some disagreement in amplitude after the first shock cell. However, both calculations greatly underpredict the shock-cell decay after the fourth cell. It is believed that the flow did not reach steady state, and the measurement after the fourth shock cell is the representations of time average flows. It is believed that the disagreements with experiments are related to the limitations of the PNS methodology to handle the elliptic effects.

(See the Appendix for the flux-Jacobians $J_1^{\pm}$, $J_2^{\pm}$, $J_3^{\pm}$, and V_2

The implicit upwing/relaxation algorithm of Newsom et. al (Ref. 1) is used to solve TLNS equations. This can be achieved through a series of alternative sweeps in the streamwise direction. For a forward sweep, $\Delta Q_{J-1,k,l}$ is known and $\Delta Q^{n+1}_{j+1,k,l}$ is set to zero. For a backward sweep, $\Delta_{j+1,k,l}$ is known and $\Delta Q_{j-1,k,l}$ is set to zero.

Finally, equations (14) is approximately factored and can be written in the following compact form:

$$(M + \delta_\eta \frac{\partial \hat{F}}{\partial Q}) M^{-1} (M + \delta_\zeta \frac{\partial \hat{G}}{\partial Q}) \Delta Q^{n+1} = R.H.S. \qquad (15)$$

where,

$$M = \frac{IVol}{\Delta t} + B_\xi$$

In the present code, the PNS equations are solved by retaining the time dependent terms and the steady state solution can be obtained by local iteration. This will allow the use of the same upwind flux-split procedure described in this section. Otherwise, very complicated flux-split procedure will be required because of the complex eigen-values and eigen-vectors of the steady state equations. At each cross-plane, local integration is used until the R.H.S. of equation (15) is reduced by 4-order of magnitude. Then, this solution is used as an initial condition for the next cross-sectional plane. This procedure is repeated for each cross-sectional plane cepta ξ_{max}

THE BOUNDARY CONDITIONS

Figure (2) shows a typical physical domain, used in the present study. The figure also shows the different boundary associated with external flow proplem.

1) Inlet Flow Conditions at $\xi = 0.$ $(z = 0)$

The static pressure, P. stream wise velocity, w, and temperature, are extracted form the measurement of Norum and Seiner (Ref. 14). The values of X- velocity, u, and y-velocity, v, are set to zero. Then, density ρ satisfies the equation of state

$$\rho = P/R_g\theta \tag{16}$$

and

$$E_t = \frac{P}{\gamma - 1} + \frac{1}{2}\rho\ (u^2 + v^2 + w^2) \tag{17}$$

which is used to calculate the total energy, E_t.

2) Conditions at ζ_o or $\zeta = 0.$ $(x = 0.)$

Factitious grid points are located along the side of ζ line as shown in figure (3). The points are denoted by subscript f, and their values are obtained from the following relations,

Figure (11) shows the comparisons between 3-D PNS and TLNS (1000 and 2000 time steps) solutions for the sonic jet with pressure ratio of 1.61. The first 3 shock cells did not show any significant differences for the PNS and TLNS solutions. It is clear that the flow is unstable and will not reach a steady state. Figure (12) shows the density and pressure contours for the same results shown in figure (11). In this figure, the PNS and TLNS predict similar shock cell structure for the first 3 shock cells. For the TLNS solution, the first three shock cell seem to be quite stable and their structure is completely time independent. Close to the third shock cell a nearly normal shock is formed and it interacts with the basic structure. The flow beyond this point is completely unstable and vortex rings are formed on the jet boundary of the entire flow field. The same obsrervations were made by Matsuda et. al. (Ref. 17). Matsuda et. al. 17 investigated, experimentally and theoretically, the decay of the shock cell structure for a sonic jet with pressure ratio of 2. They took two kinds of Schieren photographs, a long time exposure (1/30s) and and short time exposrue (1/1000s). With a short time exposure, they observed that the flow is turbulent with vortices (unstable).
On the other hand, the long time exposure gives a rather regular and smooth shock cell structure.

SUMMARY

The development of PAB3D PNS and TLNS codes and their application to nonaxisymmetric jet mixing problem are described in this report. These codes were compared with the experimental data for underexpanded supersonic jets exhausting into a subsonic external stream. The PNS code successfully predicts the shock cell structure of Mach 2.0 jet as compared with the TLNS code results. The PNS calculations were completed in less than 3 percent of

the TLNS computational time. However, PNS code fails to predict the flow field of strongly resonant jet (sonic case) beyond the first three shock cells. This was expected as the flow beyond this point was completely unstable and the only way to simulate this kind of flow is through the use of time dependent codes. For this kind of flow problem, the static or total pressure measurements should be accompanied by Schlieren photographs of a short and long time exposure or any method which can show the flow time dependency.

In general, the PNS code can simulate efficiently, mildly underexpanded and fully supersonic flow problems, and can be used to set the initial conditions for a time dependent code. On the other hand, the TLNS can handle relatively complicated flow problems. The developments of these codes should be followed by a detailed validation study using nonaxisymmetric jet mixing data base. Right now, the TLNS code is currently being modified to include a multi-zone option which will give it the capability to simulate nozzle/afterbody/jet exhaust problems including vertical and horizontal tails.

REFERENCES

1. Newsome, R. W.; Walters, R. W.; and Thomas, J. L.: An Efficient Iteration Strategy for Upwind/Relaxation Solutions to the Thin-Layer Navier-Stokes Equations. AIAA Paper 87-1113, 1987.
2. Von Glahn, U. H.: Two-Dimensional Nozzle Plume Characteristics. AIAA Paper 87-2111, 1987.
3. Von Glahn, U. H.: Secondary Stream and Exitation Effects on Two-Dimensional Nozzle Plume Characteristics. AIAA Paper 87-2112, 1987.
4. Capone, F. J.: Summary of Propulsive-Lift Research in the Langley 16-Foot Transonic Tunnel. Journal of Aircraft, Vol. 13, no. 10, October. 1976, pp. 803-808.

5. Hiley, P. E.; Wallace, H. W.; and Booz, D. E.: Nonaxisymmetric Nozzles Installed in Advance Fighter Aircraft. Journal of Aircraft, Vol. 13, no. 12, December 1976.

6. Berrier, B. L., Placza, J. L.; and Richard, G. K.: Nonaxisymmetric Nozzle Technology program - An Overview. AIAA Paper 77-1225, 1977.

7. Capone, F. J.: The Nonaxisymmetric Nozzle - It Is for Real. AIAA paper 79-1810, 1979.

8. Stevens, H. L., Thayer, E. B.; and Fullerton, J. F.: Development of the Multi-Function 2-D/C-D Nozzle. AIAA Paper 81-1491, 1981.

9. Miller, E. H.; and Protopapas, J.: Nozzle Design and Integation in an Advanced Supersonic Fighter. AIAA Paper 79-1813, 1979.

10. Dash, S. M.; and Wolf, D. E.: Fully-Coupled Analysis of Jet Mixing Problems, Part I: Shock-Capturing Model, SCIPVIS, NASA CR-3761, January 1984.

11. Dash, S. M.; Wolf, D. E.; Shinha, N.; and Lee, S. H.: Progress in the Development of Parabolized Navier-Stokes (PNS) Methodology for Analyzing Propulsive Jet Mixing Problems. AIAA Paper 86-1115, 1986.

12. Wolf, D. E.; Sinha, N.; and Dash, S. M.: Fully-Coupled Analysis of Jet Mixing Problems: Three-Dimensional PNS Model, SCIP3D. NASA CR-4139, 1988.

13. Seiner, J. M.: Advances in High Speed Jet Acoustics. AIAA Paper 84-2275, 1984.

14. Norum, T. D. and Seiner, J. M.: Measurements of Mean Static Pressure and Far-Field Acoustics of Shock-Containing Supersonic Jets. NASA TM-84521, 1982.

15. Seiner, J. M.; Dash, S. M.; and Wolf, D. E.: Shock Noise Features Using the SCIPVIS Code. AIAA Paper 83-0705, 1983.

16. Abdol-Hamid, K. S. and Wilmoth, R. G.: Multiscale Turbulence Effects in Underexpanded Supersonic Jets. AIAA Paper 87-1377, 1987.

17. Matsuda, T.; Umeda, Y.; Ishii, R.; Yasuda, A.; and Sawada, K.: Numerical and Experimental Studies on Choked Underexpanded Jets. AIAA Paper 87-1378, 1987.

18. Cline, M. C.: VNAP2: A Computer Program for Computation of Two-Dimensional, Time-Dependent, Compressible, Turbulent Flow. Los Alamos National Laboratory Report LA-8872, August 1981.

19. Chakravarthy, S. R. and Szema, K. Y.: An Euler Solver for Three-Dimensional Supersonic flows with Subsonic Pockets. AIAA Paper 85-1703, 1985.

20. Vingeron, Y. C., Rakich, J. V., and Tannehill, J. C.: Calculation of Supersonic Viscous Low Over Delta Wings with Sharp Subsonic Leading Edges. AIAA Paper 78-1137, 1978.

21. van Leer, B.: Flux-Vector Splitting for the Euler Equations. ICASE Report 82-30, 1982.

22. Norum, T. D. and Shearin, J. G.: Shock Structure and Noise of Supersonic Jets in Simulated Flight to Mach 0.4. NASA TP-2785, 1988.

APPENDIX

This appendix decribes in detail the Jacobians of the PNS and TLNS governing equations for the inviscid and viscous terms

1) Inviscid Flux-Jacobians

$$J_1^{\pm} = \frac{\partial \hat{E}_i^{\pm}}{\partial Q} \ , \ J_2^{\pm} = \frac{\partial \hat{F}_i^{\pm}}{\partial Q} \text{ and } J_3^{\pm} = \frac{\partial \hat{G}_i^{\pm}}{\partial Q}$$

a) Supersonic $|M_\xi| > |$

$M_\xi > 1 \qquad J_1^- = 0 \quad , \quad J_1^+ = \frac{\partial \hat{E}_1}{\partial Q}$

$M_\xi < 1 \qquad J_1^+ = 0 \quad , \quad J_1^- = \frac{\partial \hat{E}_i}{\partial Q}$

$$
J_1^{\pm} = \begin{bmatrix}
0 & S_x & S_y & S_z & 0 \\
\omega S_x \phi - \Omega u & \Omega - S_x\,[\omega(\gamma - 1) - 1]u & S_y u - S_x \omega(\gamma - 1)v & S_z u - S_x \omega(\gamma - 1)w & S_x \omega(\gamma - 1) \\
\omega S_y \phi - \Omega v & S_x v - S_y \omega(\gamma - 1)u & \Omega - S_y[\omega(\gamma - 1) - 1]v & S_z v - S_y \omega(\gamma - 1)w & S_y \omega(\gamma - 1) \\
\omega S_z \phi - \Omega w & S_x w - S_z \omega(\gamma - 1)u & S_y w - S_z \omega(\gamma - 1)v & \Omega - S_z[\omega(\gamma - 1) - 1]w & S_z \omega(\gamma - 1) \\
(\phi - D_1)\Omega & S_x D_1 - (\gamma - 1)\Omega u & S_y D_1 - (\gamma - 1)\Omega v & S_z D_1 - (\gamma - 1)\Omega w & \gamma\Omega
\end{bmatrix}
$$

The above matrix was used for PNS and NS calculations. For PNS calculations, ω is evaluated using eq. (4) and J_- vanishes. On the other hand, ω is set to value of 1 for the SNS calculations.

where

$$\phi = \frac{\gamma - 1}{2}(u^2 + u^2 + w^2) \ , \ \bar{U} = S_x u + S_y u + S_z w$$

$$D_1 = (E_t + p)/\rho$$

b) Subsonic for SNS Solutions $|M_\xi| < 1$

$$J_1^{\pm}(1,1) = \frac{S}{4}(1 - M_\xi^2)(a + \rho D_3)$$

$$J_1^{\pm}(1,2) = -D_4 D_2 u + S_x D_5$$

$$J_1^{\pm}(1,3) = -D_4 D_2 v + S_y D_5$$

$$J_1^{\pm}(1,4) = -D_4 D_2 w + S_z D_5$$

$$J_1^{\pm}(1,5) = D_4 D_2$$

$$J_1^{\pm}(2,1) = J_1^{\pm}(1,1) D_{12} \pm 2 s_x \rho D_6 D_3 + \gamma(s_x D_7 - u) D_6$$

$$J_1^{+}(2,2) = J_1^{+}(1,2) D_{12} \mp 2 s_x \rho D_6 D_2 u + \gamma(1 - s_x^2) D_6$$

$$J_1^{\pm}(2,3) = J_1^{\pm}(1,3) D_{12} \mp 2 s_x \rho D_6 D_2 v - s_x s_y D_6$$

$$J_1^{\pm}(2,4) = J_1^{\pm}(1,4)\, D_{12} \mp 2s_x \rho D_6 D_2 w - s_x s_z D_6$$

$$J_1^{\pm}(2,5) = J_1^{\pm}(1,5) D_{12} \pm 2s_x \rho D_6 D_2$$

$$J_1^{\pm}(3,1) = J_1^{\pm}(1,1)\, D_{13} \pm 2\, s_y \rho D_6 D_3 + \gamma(s_y D_7 - u) D_6$$

$$J_1^{\pm}(3,2) = J_1^{\pm}(1,2) D_{13} \mp 2s_y \rho D_6 D_2 u - s_x s_y D_6$$

$$J_1^{\pm}(3,3) = J_1^{\pm}(1,3) D_{13} \mp 2s_y \rho D_6 D_2 v + \gamma D_6 (1 - s_y^2)$$

$$J_1^{\pm}(3,4) = J_1^{\pm}(1,4)\, D_{13} \mp 2s_y \rho D_6 D^2 w - s_y s_2 D_6$$

$$J_1^{\pm}(3,5) = J_1^{\pm}(1,5) D_{13} \pm 2s_y \rho D_6 D_2$$

$$J_1^{\pm}(4,1) = J_1^{\pm}(1,1)\, D_{14} \pm 2s_z \rho D_6 D_3 + \gamma(s_z D_2 - w)\, D_6$$

$$J_1^{\pm}(4,2) = J_1^{\pm}(1,2)\, D_{15} \mp 2s_z \rho D_6 D_2 u - s_z s_x D_6$$

$$J_1^{\pm}(4,3) = J_1^{\pm}(1,3)\, D_{14} \mp 2s_z \rho D_6 D_2 v - s_z s_y D_6$$

$$J_1^{\pm}(4,4) = J_1^{\pm}(1,4)\, D_{14} \mp 2s_z \rho D_6 D_2 w + \gamma D_6$$

$$J_1^{\pm}(4,5) = J_1^{\pm}(1,5)\, D_{14} \pm 2s_z \rho D_6 D_2$$

$$J_1^{+}(5,1) = J_1^{*}(1,1)\, D_{15} + (D_8 D_3 + D_9 \frac{\bar{U}}{\bar{s}} - (\gamma - 1)\rho \frac{2\phi}{} D_{11}$$

$$J_1^{\pm}(5,2) = J_1^{\pm}(1,2)\, D_{15} - (D_8 D_{2u} + s_x D_q + \frac{u}{\rho})\, D_{11}$$

$$J_1^{\pm}(5,3) = J_1^{\pm}(1,3)\, D_{15} - (D_8 D_{2v} + s_y D_g + \frac{u}{\rho}\, D_{11}$$

$$J_1^{\pm}(5,4) = J_1^{\pm}(1,4)\, D_{15} - (D_8 D_{2w} + s_z D_g + \frac{w}{\rho})\, D_{11}$$

$$J_1^{\pm}(5,5) = J_1^{\pm}(1,5)\, D_{15} - D_\rho D_2\, D_{11}$$

$$D_2 = \frac{\gamma(\gamma - 1)}{2\rho a}\ ,\ D_3 = D_2\,(\frac{2\phi}{\gamma - 1} - \frac{E_t}{\rho})\ ,\ D_4 = \frac{S}{4}\,\rho\,(1 - M_\xi^2)$$

$$D_5 = \frac{1}{2}\,(1 \pm M_\xi)\ ,\ D_6 = \frac{\hat{E}_i^{\pm}(1)}{\gamma\rho}\ ,\ D_7 = \frac{\bar{U}}{\gamma}$$

$$D_8 = \frac{4a}{\gamma^2 - 1} \pm \frac{2}{\gamma + 1}\,\frac{\bar{U}}{S}\ ,\ D_g = \frac{2}{\gamma + 1}\ \ (\frac{\bar{U}}{S} \pm a)/\rho$$

$$D_{11} = \hat{E}_i^{\pm}(1),\ D_{12} = \frac{\hat{E}_i^{\pm}(2)}{D_{11}}\ ,\ D_{13} = \frac{\hat{E}_i^{\pm}(3)}{D_{11}}$$

$$D_{14} = \frac{\hat{E}_i^{\pm}(4)}{D_{11}} \text{ and } D_{15} = \frac{\hat{E}_i^{\pm}(5)}{D_{11}}$$

For the η direction, flux - Jacobian $(J_2^{\pm})$,

$$\omega = 1 \quad M_\xi \to M_\eta\ ,\ \bar{U} \to \bar{V}\ ,\ \begin{matrix} S \\ \xi \end{matrix} \to \begin{matrix} R \\ \eta \end{matrix} \text{ and } \hat{E}_i^{\pm} \to \hat{F}_i^{\pm}$$

For the ζ direction Flux-Jacobian ($J_3^{\pm}$),

$$\omega = 1 \quad M_{\xi} \rightarrow M_{\eta} \ , \ \bar{U} \rightarrow \bar{W} \ , \ \begin{matrix} S \rightarrow T \\ s \rightarrow t \end{matrix} \text{ and } \hat{E}_i^{\pm} \rightarrow \hat{G}_i^{\pm}$$

2) Viscous Flux-Jacobians

Neglecting cross-derivative term, the viscous flux vector in the η is given by:

$$\hat{F}_v = \frac{m}{Vol} \begin{matrix} 0 \\ R_x \bar{U}_{\eta} + R^2 u_{\eta} \\ R_y \bar{U}_{\eta} + R^2 v_{\eta} \\ R_z \bar{U}_{\eta} + R^2 w_{\eta} \end{matrix}$$

$$R^2 \phi_{\eta} + \hat{U}_{\eta} + \frac{1}{3} R_x R_y (uv)_{\eta} + R_y R_z (vw)_{\eta} + R_z R_x (wu)_1 + \frac{R^2}{(\gamma - 1) P_r} (a^2)_{\eta}$$

where, Vol is the cell volume,

$$\bar{U}_{\eta} = \frac{1}{3} (R_x u_{\eta} + R_y v_{\eta} + R_z w_{\eta}) \ , \ \hat{U}_{\eta} = \frac{1}{6} R_x^2 (u^2)_{\eta} + R_y^2 (v^2)_{\eta} + R_z^2 (w^2)_{\eta}$$

and $$\phi_{\eta} = \frac{1}{2} (u^2)_{\eta} + (v^2)_{\eta} + (w^2)_{\eta}$$

The viscous flux vector in the ξ direction can be constructed by replacing the following variables in the above formulas,

$$\hat{F}_v \to \hat{G}_v \ , \ \hat{R} \to \hat{T}_{\eta \to \zeta} \text{ and } \hat{R} = [R_x, R_y, R_z]^T$$

The viscous flux-Jacobian is given as follows:

$$\frac{\partial F_v\ (R_{k1}\ ,\ Q_{k2})}{\partial Q_{k2}} = V_2\ (k_1,\ k_2)$$

for $k_1 = k + 1/2$, $k_2 = k + 1$ & k

$k_1 = k - 1/2$, $k_2 = k$ & $k - 1$

Then,

$$V_2(k_1 k_2) = \frac{\mu}{\rho \overline{Vol}} \begin{Bmatrix} 0 & 0 & 0 & 0 & 0 \\ -(R_x \bar{U} + R^2 u) & R^2 + \frac{1}{3} R_x^2 & \frac{1}{3} R_y R_x & \frac{1}{3} R_z R_x & 0 \\ -(R_y \bar{U} + R^2 v) & \frac{1}{3} R_y R_x & R^2 + \frac{1}{3} R_y^2 & \frac{1}{3} R_y R_z & 0 \\ -(R_z \bar{U} + R^2 w) & \frac{1}{3} R_z R_x & \frac{1}{3} R_z R_y & R^2 + \frac{1}{3} R_z^2 & 0 \\ -[R^2(2 - \frac{\gamma}{P_r})\ \phi + \hat{U} & R^2 u + R_x \bar{U} & R^2 v + R_y \bar{U} & R^2 w + R_z \bar{U} & \frac{\gamma R^2}{P_r} \\ +\frac{2}{3}\ (R_x R_y uv + R_y R_z vw + R_z R_x wu) & -\frac{\gamma R^2 u}{P\gamma} & \frac{-\gamma R^2 v}{P_r} & \frac{-\gamma R^2}{P_r} w & \\ +\frac{R^2 a^2}{(\gamma - 1) P_r} & & & & \end{Bmatrix}$$

where,

$$\hat{U} = \frac{1}{3}\ R_x^2\ u^2 + R_y^2\ v^2 + R_2^2\ w^2\ ,$$

and $\phi = \frac{1}{2}\ (u^2 + v^2 + w^2)$

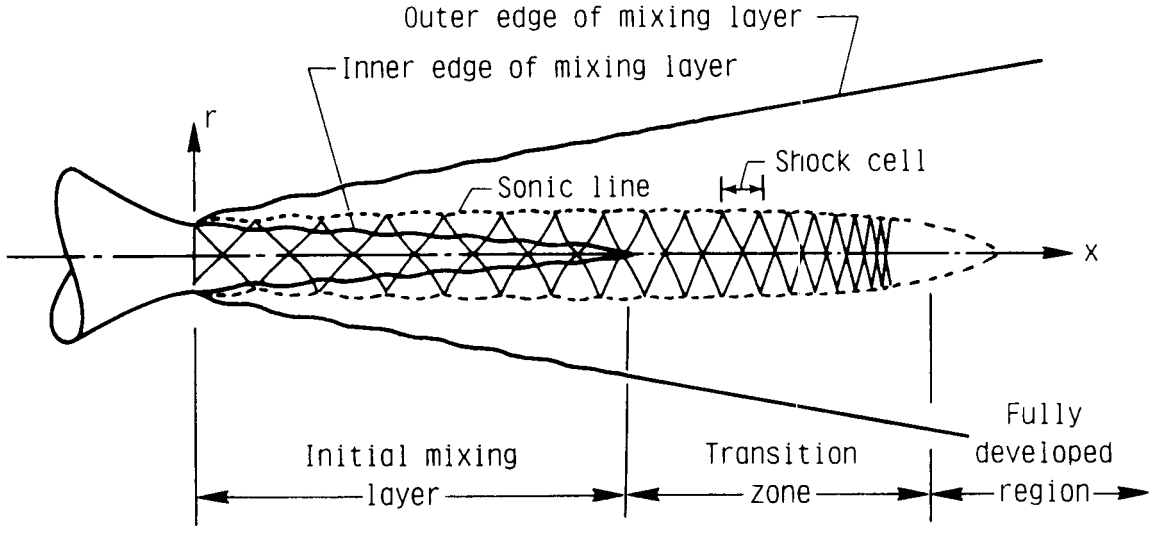

Figure 1. Typical flow field for underexpanded supersonic jet.

Figure 2. Typical grid distribution for the physical domain.

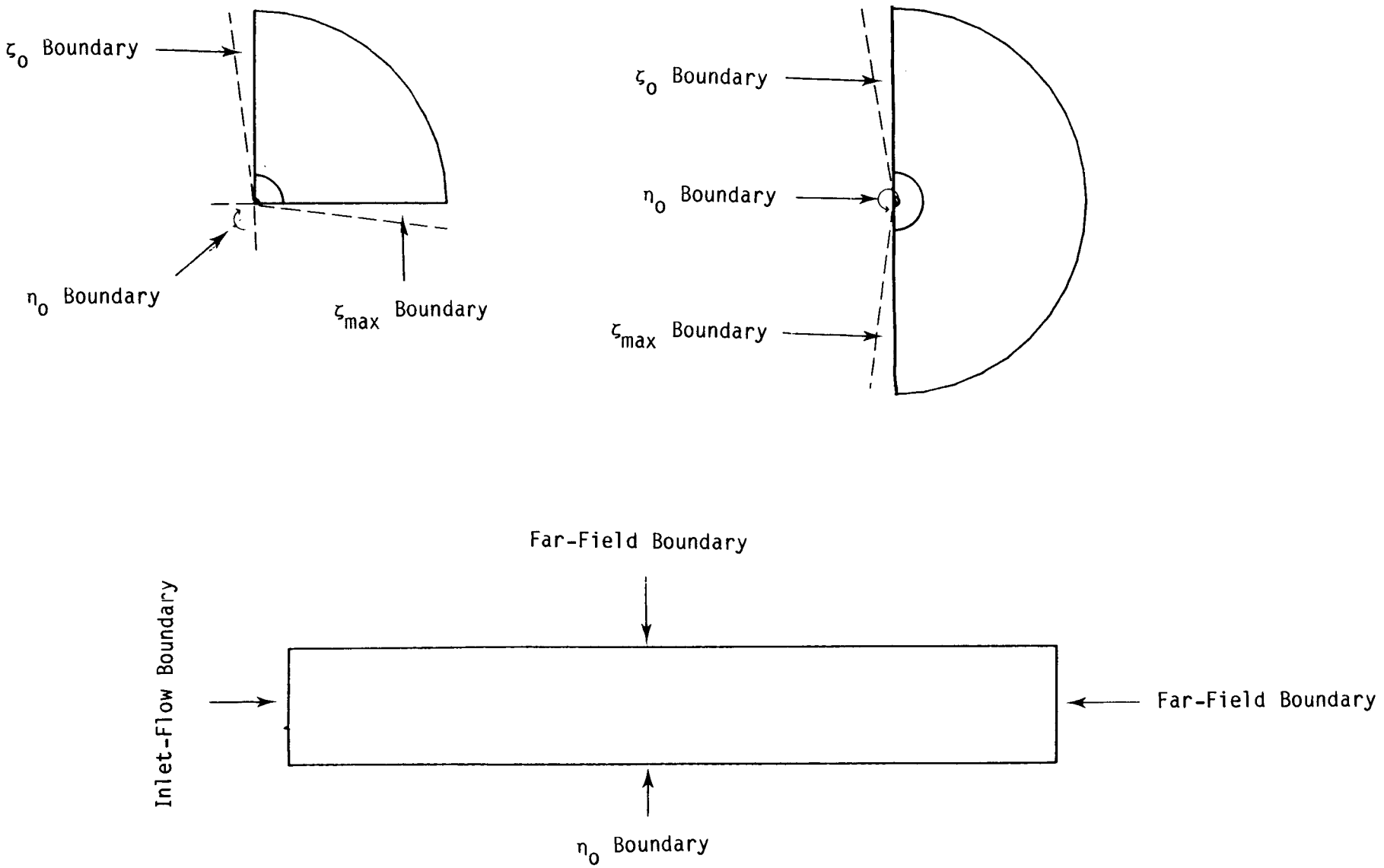

Figure 3. Boundary grid points for the jet cross-sectional plane.

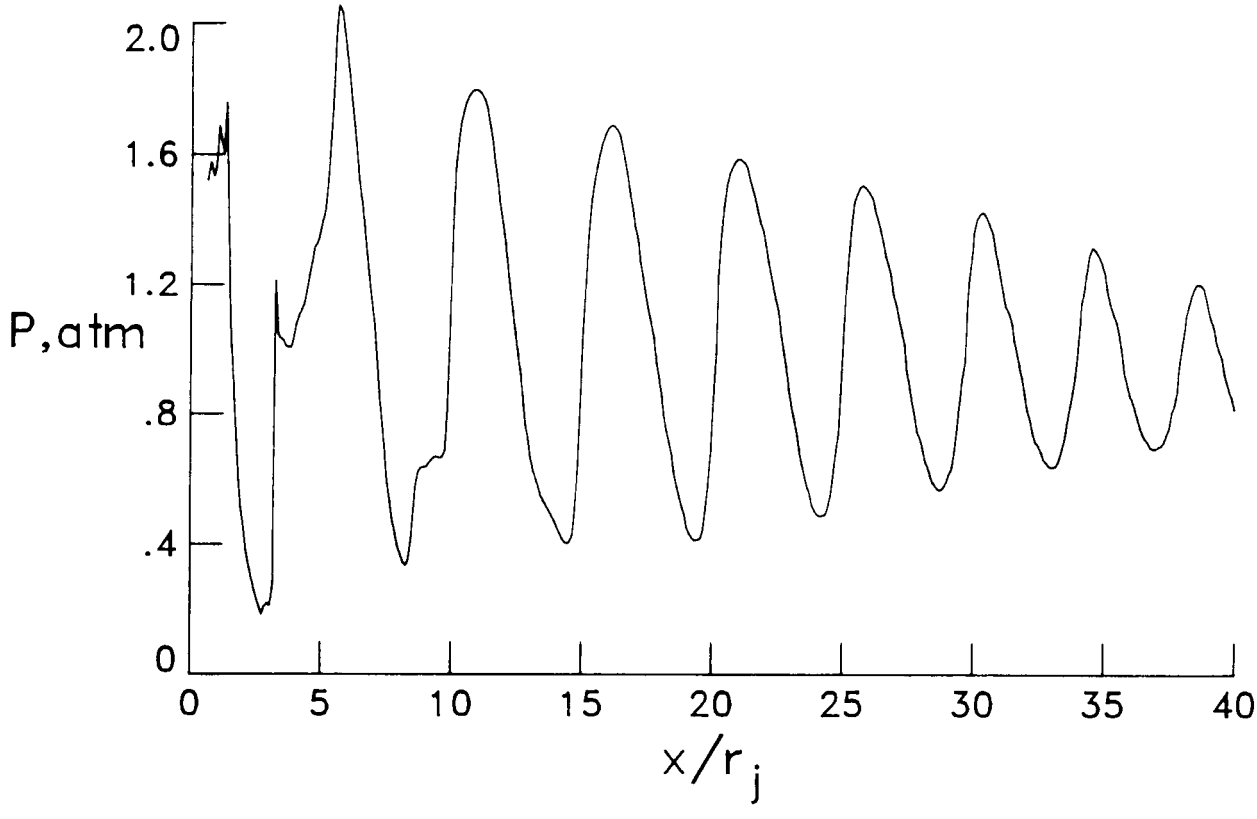

Figure 4. Measured plume centerline pressure for underexpanded supersonic jet. (Data from ref. 14)

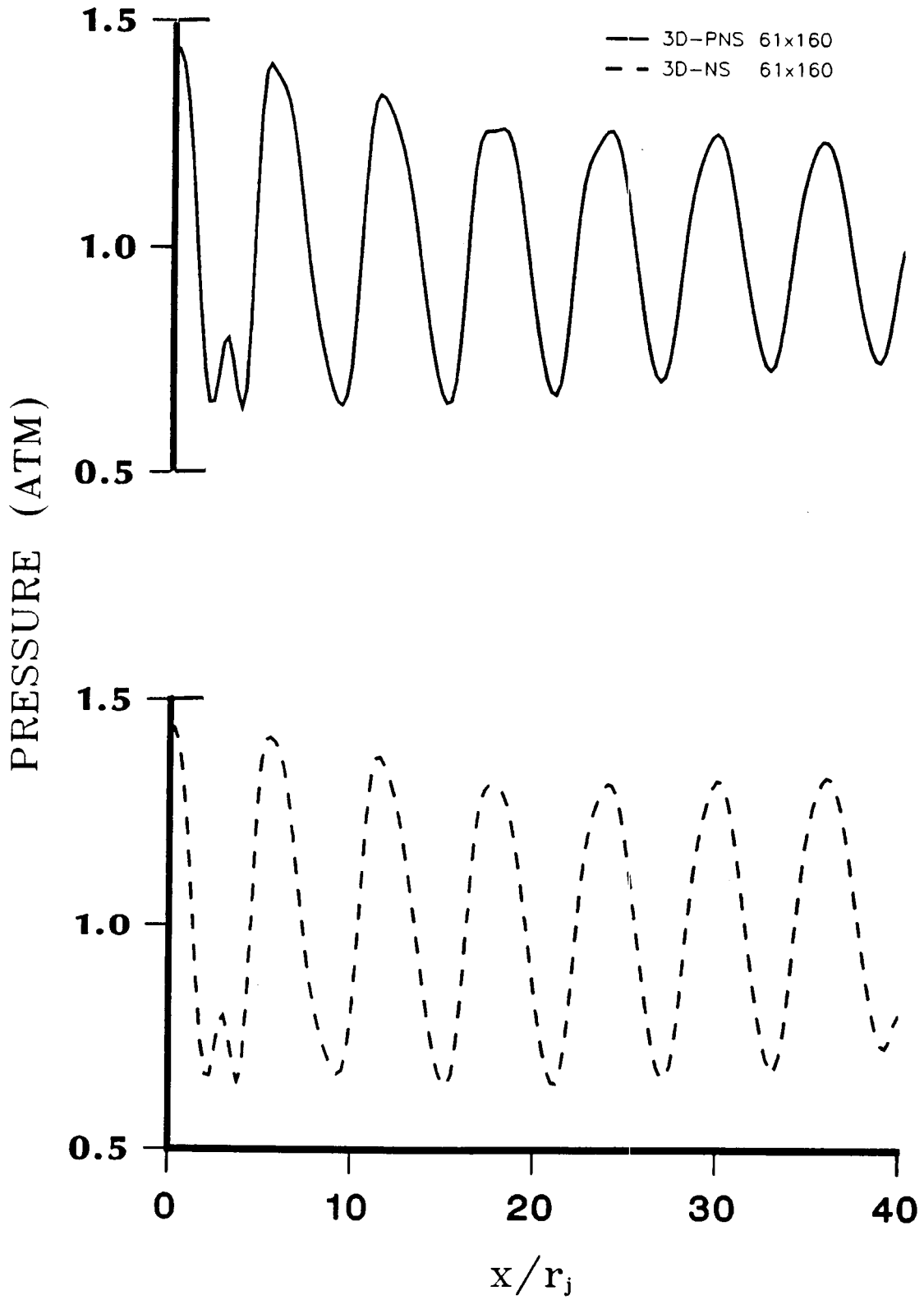

Figure 5. Comparison of 3-D PNS and 3-D NS predicted centerline pressures for underexpanded supersonic jet.

A) PNS SOLUTION

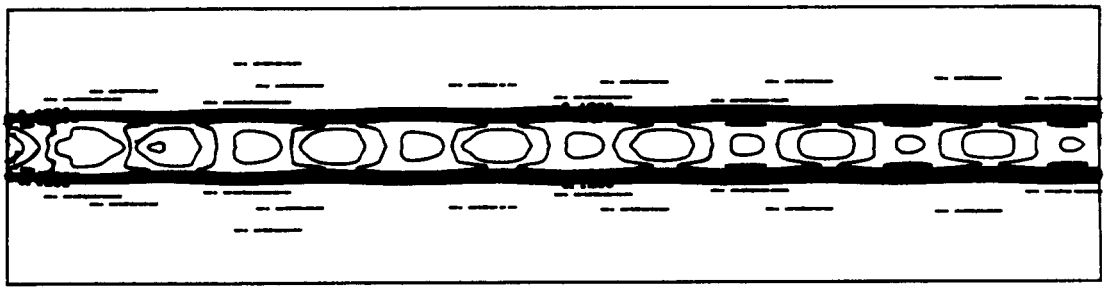

DENSITY CONTOUR *CONTOUR INTERVAL = .11900E+00*

B) NS SOLUTION

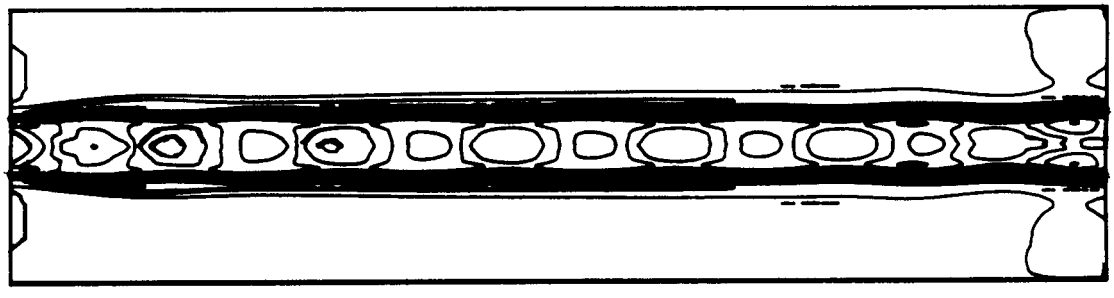

DENSITY CONTOUR *CONTOUR INTERVAL = .11942E+00*

Figure 6a. Comparison of 3-D and 3-D PNS predicted density contours for underexpanded supersonic jet.

A) PNS SOLUTION

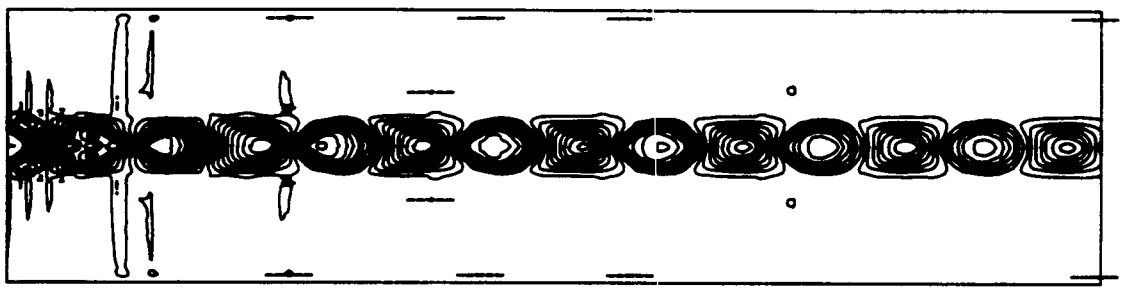

PRESSURE CONTOUR *CONTOUR INTERVAL = .37381E+04*

B) NS SOLUTION

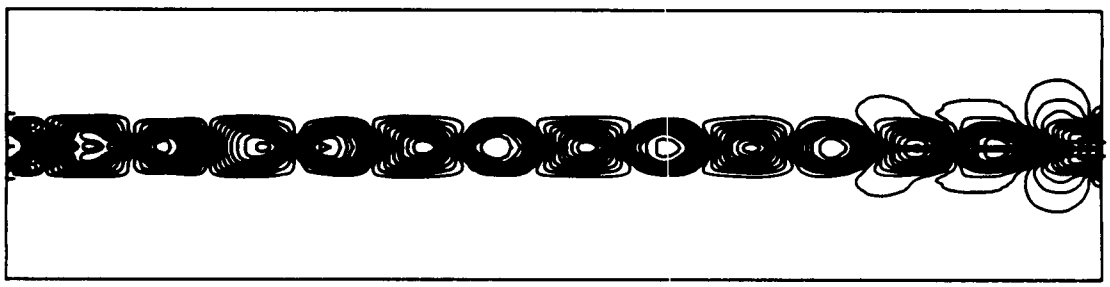

PRESSURE CONTOUR *CONTOUR INTERVAL = .37929E+04*

Figure 6b. Comparison of 3-D and 3-D PNS predicted pressure contours for underexpanded supersonic jet.

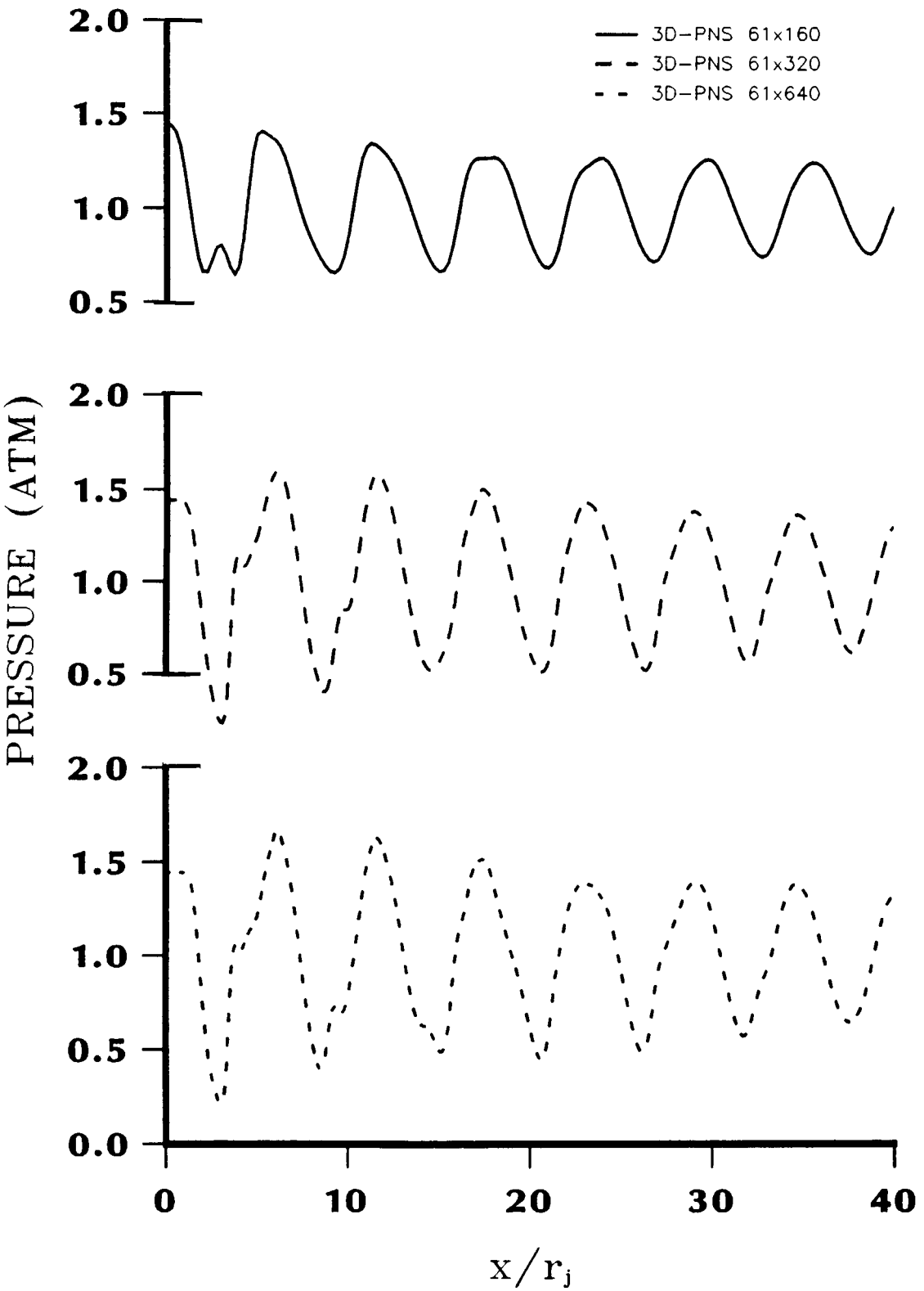

Figure 7. Comparison of 3-D PNS predicted centerline pressures for underexpanded supersonic jet.

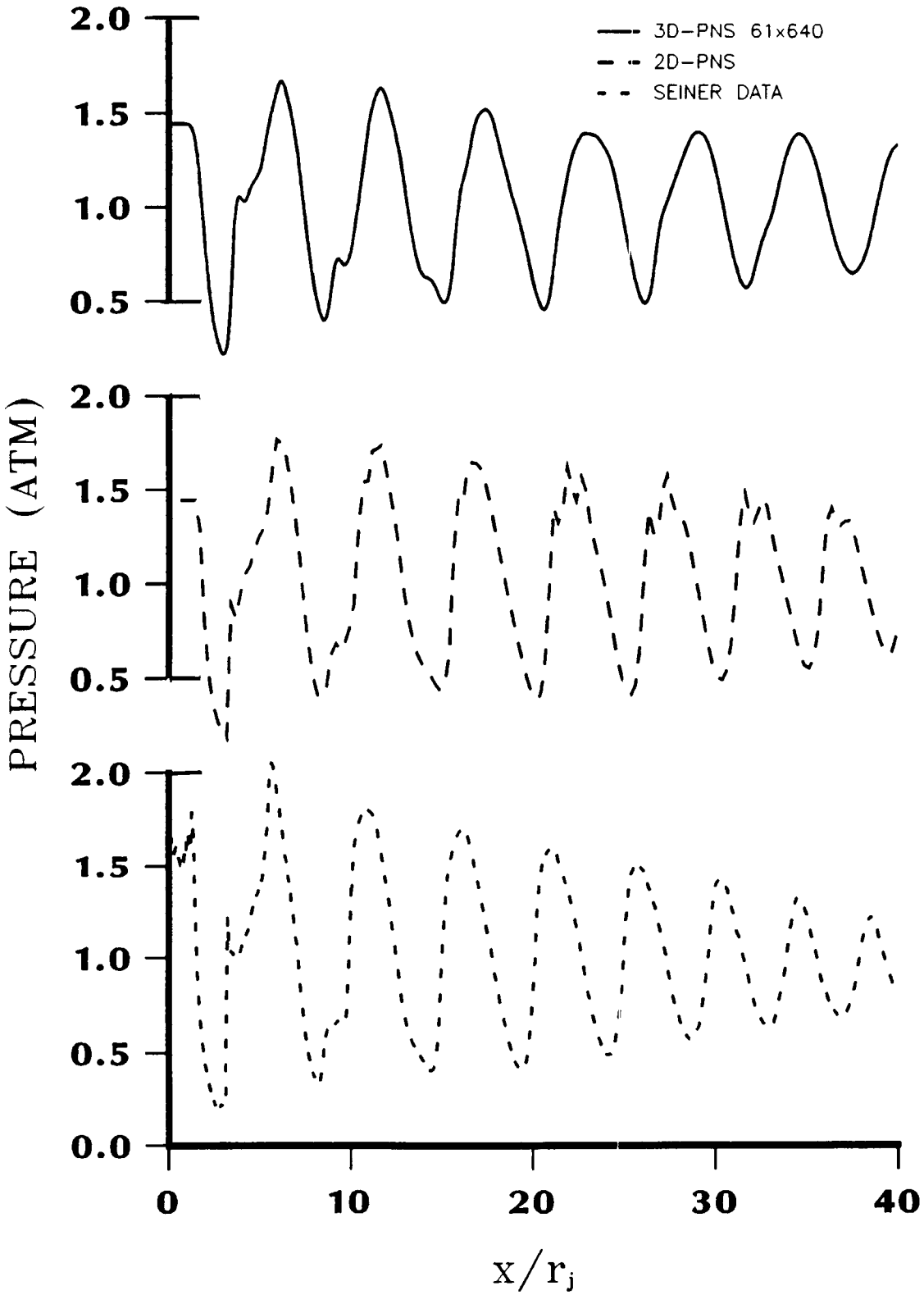

Figure 8. Comparison of predicted (2-D and 3-D PNS) and measured centerline pressure for underexpanded supersonic jet.

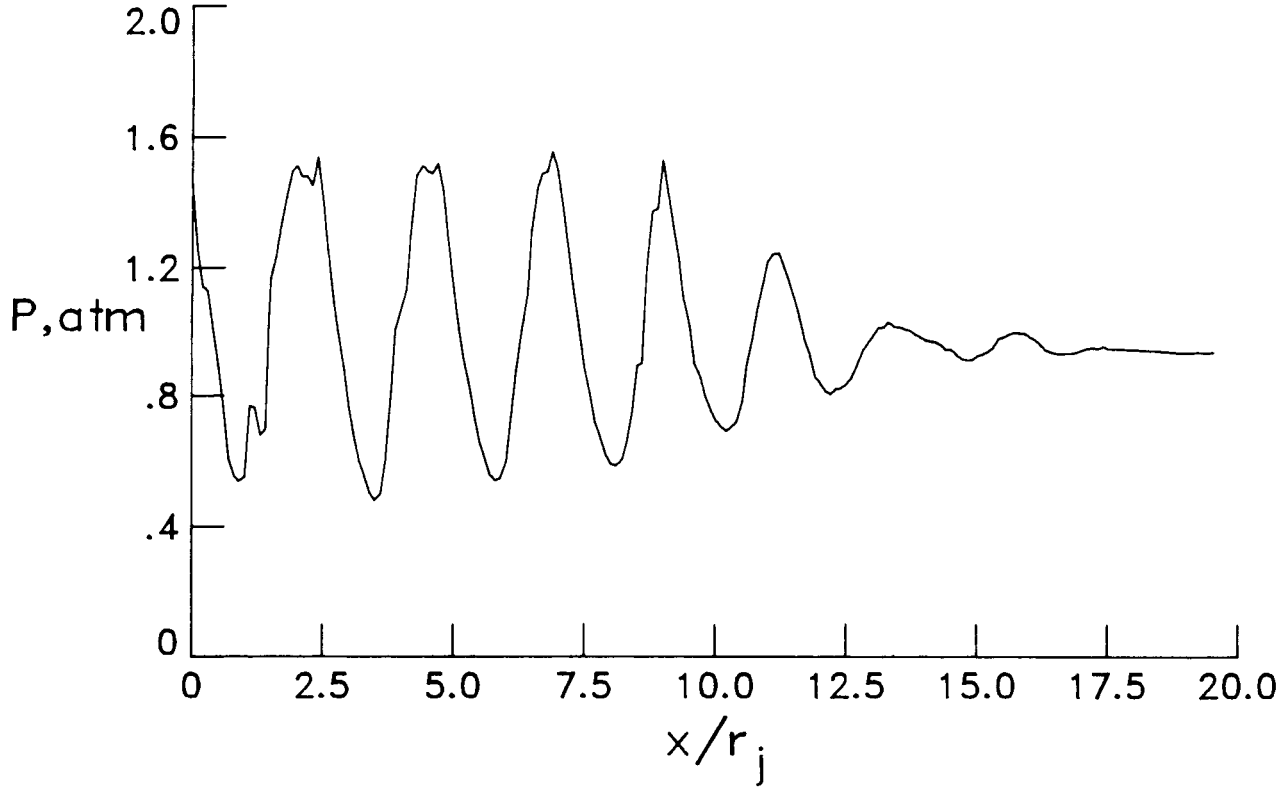

Figure 9. Measured plume centerline pressure for underexpanded sonic jet. (Data from ref. 14)

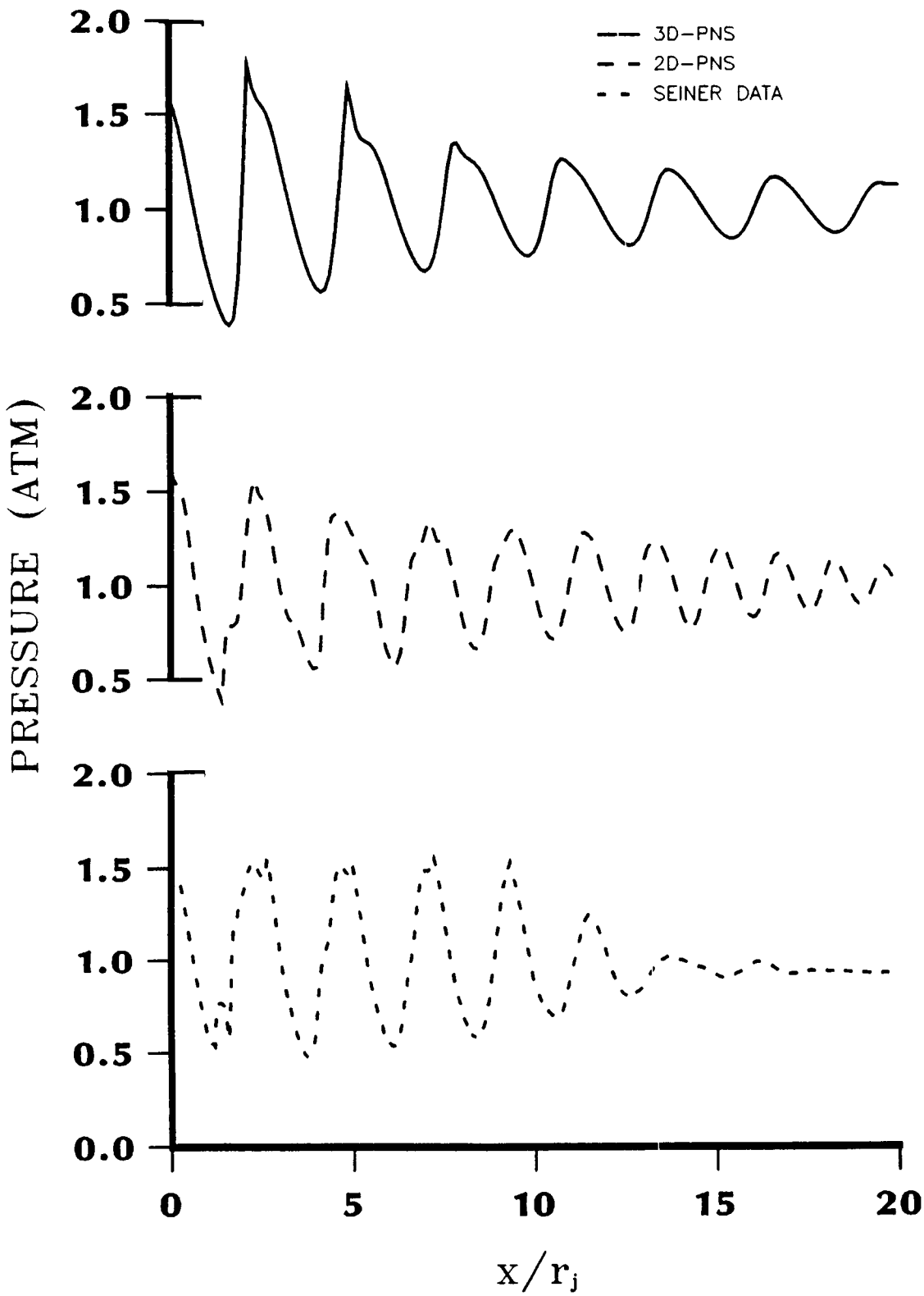

Figure 10. Comparison of predicted (2-D and 3-D PNS) and measured centerline pressure for underexpanded sonic jet.

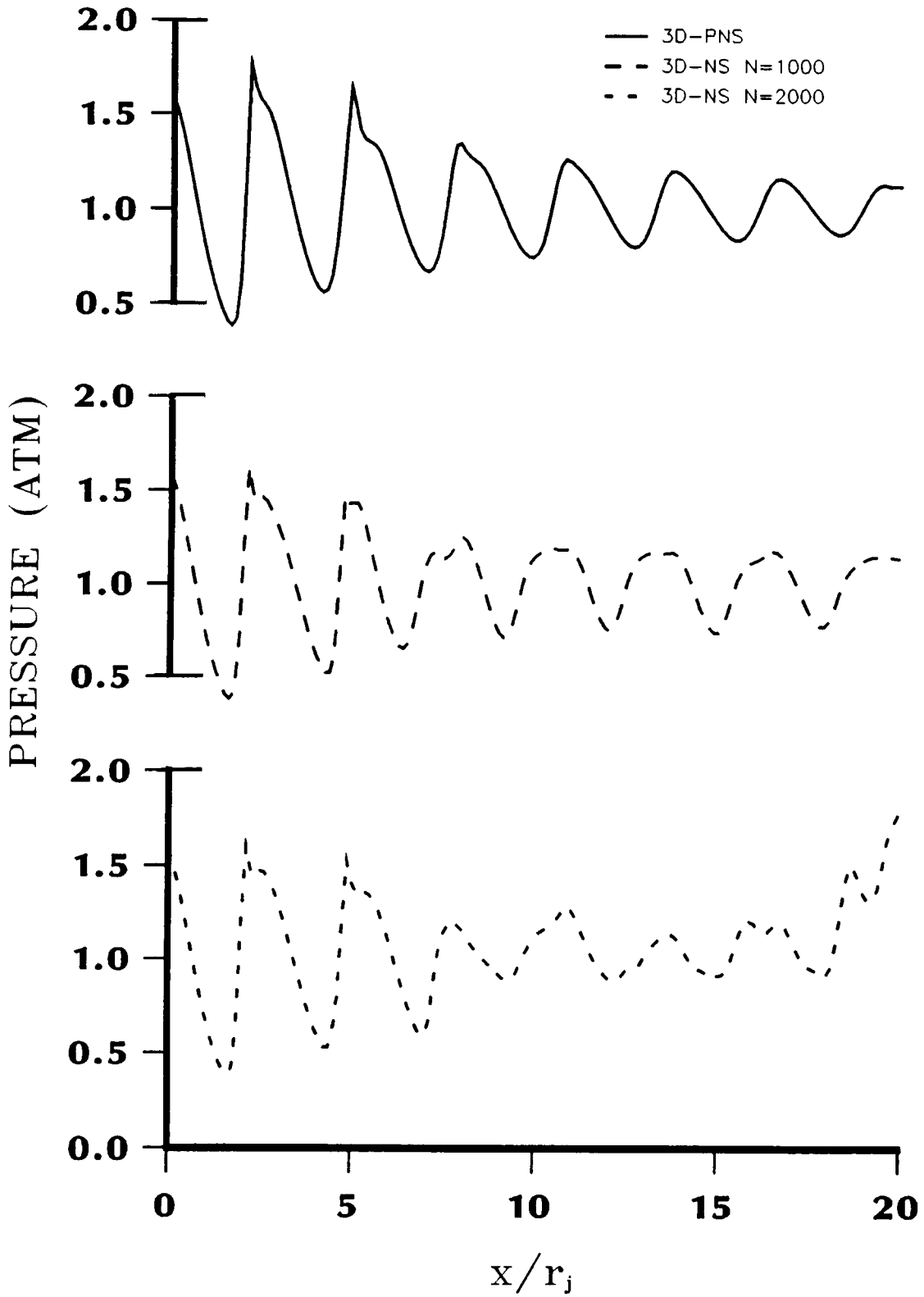

Figure 11. Comparison of 3-D and 3-D PNS predicted centerline pressures for underexpanded sonic jet.

A) PNS SOLUTION

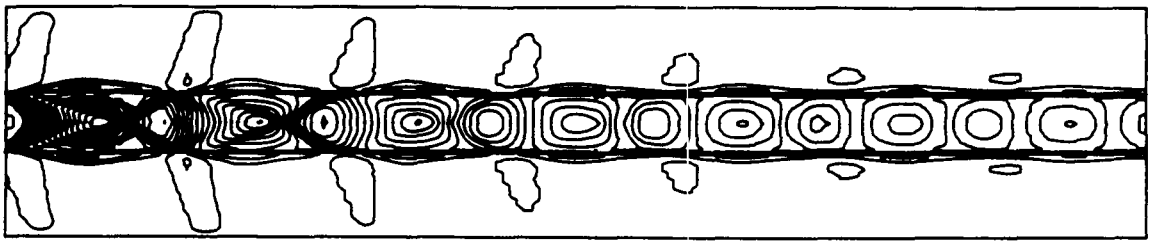

DENSITY CONTOUR CONTOUR INTERVAL = .60428E-01

B) NS SOLUTION AT N=1000

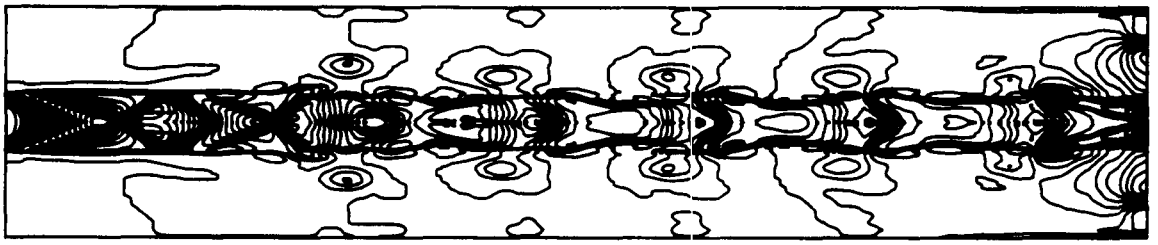

DENSITY CONTOUR COINTOUR INTERVAL = .59403E-01

C) NS SOLUTION AT N=2000

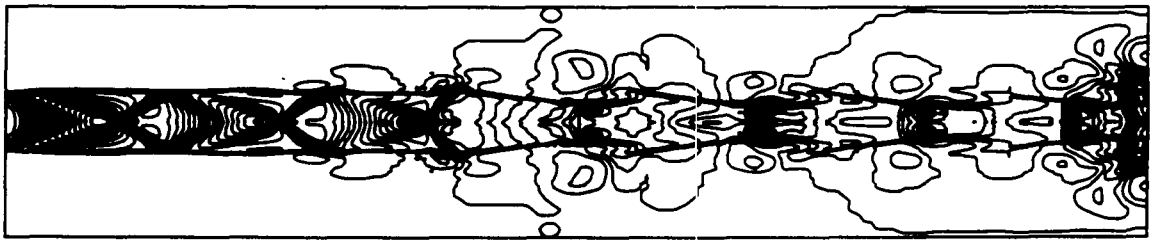

DENSITY CONTOUR CONTOUR INTERVAL = .59630E-01

Figure 12a. Comparison of 3-D and 3-D PNS predicted density contours for underexpanded sonic jet.

A) PNS SOLUTION

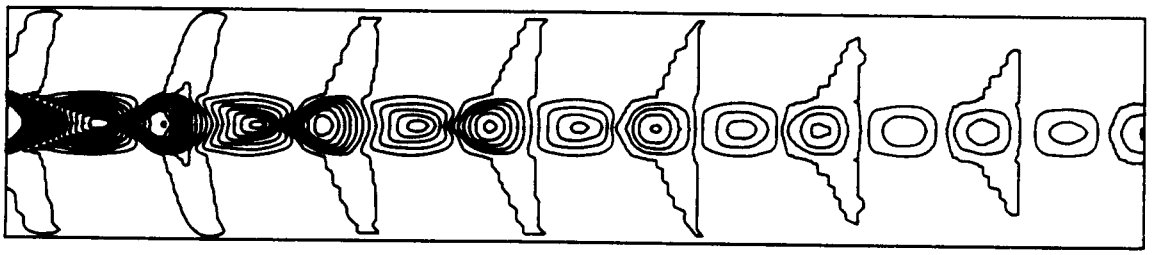

PRESSURE CONTOUR CONTOUR INTERVAL = .55477E+04

B) NS SOLUTION AT N=1000

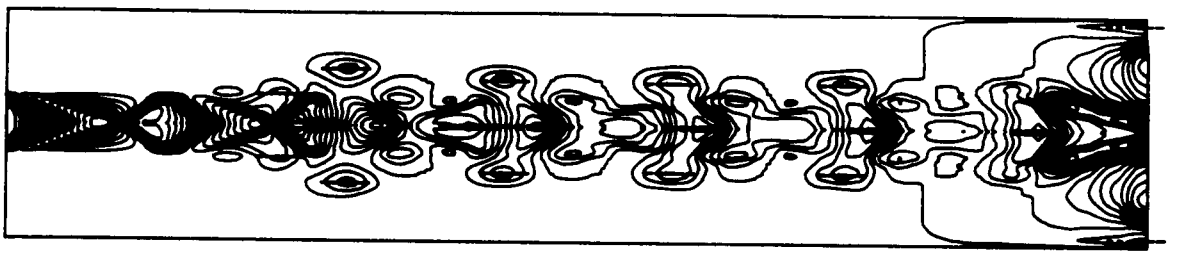

PRESSURE CONTOUR CONTOUR INTERVAL = .56548E+04

C) NS SOLUTION AT N=2000

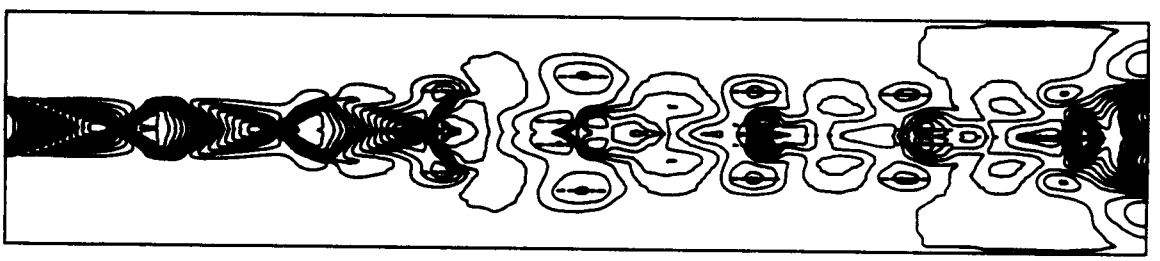

PRESSURE CONTOUR CONTOUR INTERVAL = .56613E+04

Figure 12b. Comparison of 3-D and 3-D PNS predicted pressure contours for underexpanded sonic jet.

NASA
National Aeronautics and Space Administration

Report Documentation Page

1. Report No.	2. Government Accession No.	3. Recipient's Catalog No.
NASA CR-4200		

4. Title and Subtitle
Development of Three-Dimensional Code for the Analysis of Jet Mixing Problem - Part I: Laminar Solution

5. Report Date
December 1988

6. Performing Organization Code

7. Author(s)
Khaled S. Abdol-Hamid

8. Performing Organization Report No.

10. Work Unit No.
505-62-71-01

9. Performing Organization Name and Address
Analytical Services and Materials, Inc.
107 Research Drive
Hampton, VA 23666

11. Contract or Grant No.
NAS1-18599

13. Type of Report and Period Covered
Contractor Report

12. Sponsoring Agency Name and Address
National Aeronautics and Space Administration
Langley Research Center
Hampton, VA 23665-5225

14. Sponsoring Agency Code

15. Supplementary Notes
Langley Technical Monitor: William P. Henderson

16. Abstract

Future aircraft will eventually feature nonaxisymmetric or rectangular nozzles. Developing a three-dimensional code to simulate the characteristics of the jet exhaust plume, issuing from nonaxisymmetric nozzles, in general, at different flight conditions, is very important. In the present investigation, two three-dimensional codes were developed to simulate the shock-cell structure of circular nozzles. These codes are used to solve the parabolized and simplified Navier-Stokes equations respectively. Both codes are based on a method previously developed by Newsome et al. (Ref. 1 of paper). These codes are fully vectorized on the VPS 32 at NASA Langley Research Center. The axisymmetric underexpanded supersonic jet flow problem, exhausting into still air, was used as a test case for developing an efficient three-dimensional problems and preserving crossplane symmetry of the flow downstream of the jet exit.

17. Key Words (Suggested by Author(s))	18. Distribution Statement
Three-dimensional computational code Underexpanded supersonic jet Parabolized Navier-Stokes equations Thin Layer Navier-Stokes equations Finite volume	Unclassified - Unlimited Subject Category 02

19. Security Classif. (of this report)	20. Security Classif. (of this page)	21. No. of pages	22. Price
Unclassified	Unclassified	48	A03